A Large Strain Isotropic Elasticity Model Based on Molecular Dynamics Simulations of a Metallic Glass

Noname manuscript No.
(will be inserted by the editor)

A large strain isotropic elasticity model based on molecular dynamics simulations of a metallic glass

David L. Henann · Lallit Anand

the date of receipt and acceptance should be inserted later

Abstract For an isotropic hyperelastic material, the free energy per unit reference volume, ψ, may be expressed in terms of an isotropic function $\psi = \bar{\psi}(\mathbf{E})$ of the logarithmic elastic strain $\mathbf{E} = \ln \mathbf{V}$. We have conducted numerical experiments using molecular dynamics simulations of a metallic glass to develop the following simple specialized form of the free energy for circumstances in which one might encounter a large volumetric strain $\mathrm{tr}\,\mathbf{E}$, but the shear strain $\sqrt{2}|\mathbf{E}_0|$ (with $\mathbf{E}_0$ the deviatoric part of $\mathbf{E}$) is small but not infinitesimal:

$$\begin{aligned}
&\psi(\mathbf{E}) = \mu(\mathrm{tr}\,\mathbf{E})\,|\mathbf{E}_0|^2 + g(\mathrm{tr}\,\mathbf{E}), \qquad \text{with} \\
&\mu(\mathrm{tr}\,\mathbf{E}) = \mu_{\mathrm{r}} - (\mu_{\mathrm{r}} - \mu_0)\exp\left(\frac{\mathrm{tr}\,\mathbf{E}}{\epsilon_{\mathrm{r}}}\right), \qquad \text{and} \\
&g(\mathrm{tr}\,\mathbf{E}) = \kappa_0\,(\epsilon_{\mathrm{c}})^2\left[1 - \left(1 + \frac{\mathrm{tr}\,\mathbf{E}}{\epsilon_{\mathrm{c}}}\right)\exp\left(-\frac{\mathrm{tr}\,\mathbf{E}}{\epsilon_{\mathrm{c}}}\right)\right].
\end{aligned}$$

This free energy has five material constants — the two classical positive-valued shear and bulk moduli μ_0 and κ_0 of the infinitesimal theory of elasticity, and three additional positive-valued material constants $(\mu_{\mathrm{r}}, \epsilon_{\mathrm{r}}, \epsilon_{\mathrm{c}})$, which are used to characterize the nonlinear response at large values of $\mathrm{tr}\,\mathbf{E}$. In the large volumetric strain range $-0.30 \leq \mathrm{tr}\,\mathbf{E} \leq 0.15$ but small shear strain range $\sqrt{2}|\mathbf{E}_0| \lessapprox 0.05$ numerically explored in this paper, this simple five-constant model provides a very good description of the stress-strain results from our molecular dynamics simulations.

D. L. Henann · L. Anand
Department of Mechanical Engineering
Massachusetts Institute of Technology
Cambridge, MA 02139, USA
E-mail: anand@mit.edu

1 Introduction

Consider a homogeneous body B identified with the region of space it occupies in a fixed reference configuration, and denote by $\mathbf{X}$ an arbitrary material point of B.[1] A motion of B is described by a smooth one-to-one mapping $\mathbf{x} = \boldsymbol{\chi}(\mathbf{X}, t)$, with deformation gradient given by $\mathbf{F} = \nabla\boldsymbol{\chi}$, and $J = \det\mathbf{F} > 0$. The deformation gradient admits the polar decomposition $\mathbf{F} = \mathbf{VR}$, with $\mathbf{V}$ a symmetric positive definite (left) stretch tensor, and $\mathbf{R}$ a rotation tensor. The spectral representation of $\mathbf{V}$ is $\mathbf{V} = \sum_{i=1}^{3} \lambda_i \mathbf{l}_i \otimes \mathbf{l}_i$, where $(\lambda_1, \lambda_2, \lambda_3)$ and $(\mathbf{l}_1, \mathbf{l}_2, \mathbf{l}_3)$ are, respectively, the lists of principal stretches and principal directions of $\mathbf{V}$. For an *isotropic*, *hyperelastic* material, the free energy per unit reference volume may be expressed in terms of the principal stretches as

$$\psi = \bar{\psi}(\lambda_1, \lambda_2, \lambda_3), \tag{1}$$

with $\bar{\psi}$ invariant under the permutations of the integers $(1, 2, 3)$. Corresponding to this free energy, the Cauchy stress $\mathbf{T}$ is given by

$$\mathbf{T} = J^{-1} \sum_{i=1}^{3} \lambda_i \frac{\partial\bar{\psi}(\lambda_1, \lambda_2, \lambda_3)}{\partial\lambda_i} \mathbf{l}_i \otimes \mathbf{l}_i, \quad \text{where} \quad J = \lambda_1\lambda_2\lambda_3 > 0. \tag{2}$$

With

$$\mathbf{E} \stackrel{\text{def}}{=} \ln\mathbf{V} = \sum_{i=1}^{3} E_i \mathbf{l}_i \otimes \mathbf{l}_i, \qquad E_i = \ln\lambda_i, \tag{3}$$

denoting the *logarithmic strain*, and

$$\mathbf{T}_{\text{K}} \stackrel{\text{def}}{=} J\mathbf{T} \tag{4}$$

denoting the *Kirchhoff stress*, (2) may be written as

$$\mathbf{T}_{\text{K}} = \sum_{i=1}^{3} \frac{\partial\hat{\psi}(E_1, E_2, E_3)}{\partial E_i} \mathbf{l}_i \otimes \mathbf{l}_i. \tag{5}$$

The logarithmic elastic strain $\mathbf{E}$ has the important property that

$$\operatorname{tr}\mathbf{E} = \ln J \tag{6}$$

represents a volumetric strain, and that the deviatoric part of $\mathbf{E}$ is given by

$$\mathbf{E}_0 = \ln(J^{-1/3}\mathbf{V}). \tag{7}$$

Choosing

$$I_1(\mathbf{E}) = \operatorname{tr}\mathbf{E}, \qquad I_2(\mathbf{E}) = \operatorname{tr}\mathbf{E}_0^2, \quad \text{and} \quad I_3(\mathbf{E}) = \operatorname{tr}\mathbf{E}_0^3 \tag{8}$$

[1] *Notation*: We use standard notation of modern continuum mechanics (cf., e.g., [1]). The symbols ∇ and Div denote the gradient and divergence with respect to the material point $\mathbf{X}$ in the *reference configuration*; grad and div denote these operators with respect to the point $\mathbf{x} = \boldsymbol{\chi}(\mathbf{X}, t)$ in the deformed configuration; a superposed dot denotes the material time-derivative. We write $\operatorname{sym}\mathbf{A}$, $\operatorname{skw}\mathbf{A}$, $\mathbf{A}_0$, and $\operatorname{sym}_0\mathbf{A}$ respectively, for the symmetric, skew, deviatoric, and symmetric-deviatoric parts of a tensor $\mathbf{A}$. Also, the inner product of tensors $\mathbf{A}$ and $\mathbf{B}$ is denoted by $\mathbf{A}\!:\!\mathbf{B}$, and the magnitude of $\mathbf{A}$ by $|\mathbf{A}| = \sqrt{\mathbf{A}\!:\!\mathbf{A}}$.

as a list of three independent invariants of $\mathbf{E}$, we may alternatively write the stress-strain relation (5) as

$$\mathbf{T}_{\text{K}} = \frac{\partial \tilde{\psi}(I_1(\mathbf{E}), I_2(\mathbf{E}), I_3(\mathbf{E}))}{\partial \mathbf{E}}. \tag{9}$$

Recall that in the classical linear theory of isotropic elasticity, with $\tilde{\mathbf{E}} = (1/2)(\nabla\mathbf{u} + (\nabla\mathbf{u})^{\top})$ the infinitesimal strain tensor, the free energy is taken as

$$\psi(\tilde{\mathbf{E}}) = \mu_0 |\tilde{\mathbf{E}}_0|^2 + \frac{1}{2}\kappa_0 (\operatorname{tr}\tilde{\mathbf{E}})^2, \tag{10}$$

where $\mu_0 > 0$ and $\kappa_0 > 0$ are the shear and bulk moduli. Motivated by the simple form of the expression for the strain energy of an infinitesimally-strained isotropic elastic body, one might ask whether an analogous expression, in which dependence upon the infinitesimal strain measure is replaced by dependence upon a *finite strain measure*, is capable of describing the behavior of a moderately-strained isotropic elastic body. A model of this type, using the logarithmic strain measure (3), was introduced by Hencky [2–4] and has the form

$$\psi(\mathbf{E}) = \mu_0 |\mathbf{E}_0|^2 + \frac{1}{2}\kappa_0 (\operatorname{tr}\mathbf{E})^2, \tag{11}$$

where $\mu_0 > 0$ and $\kappa_0 > 0$ are the shear and bulk moduli from the classical *infinitesimal* theory. Anand [5,6] has shown that the quadratic free energy function (11) and the corresponding stress relation,

$$\mathbf{T}_{\text{K}} = 2\mu_0 \mathbf{E}_0 + \kappa_0 (\operatorname{tr}\mathbf{E})\mathbf{1}, \tag{12}$$

are in good agreement with experiments on a wide class of materials for principal stretches ranging between 0.7 and 1.3. Importantly, since the material constants μ_0 and κ_0 are the classical elastic constants, they may be determined from experimental data at infinitesimal strains. As a consequence of these results, it appears that all moderate-strain non-linearities are incorporated in the logarithmic strain measure. Indeed, for this reasonably large range of stretches, all other commonly used strain measures (including those of Green, Almansi, Swainger, Biot), when used to generalize the classical free energy for isotropic linear elasticity (using the values of μ_0 and κ_0 determined from experimental data at infinitesimal strains), give predictions (for the elastic stress response of materials) which are in poor agreement with experiments.

More recently, guided by the *universal binding energy relation* (UBER) introduced by Rose et al. [7], Gearing and Anand [8] modified the Hencky [2–4] free energy function to account for large elastic volumetric strains. Specifically, with

$$\epsilon \stackrel{\text{def}}{=} \operatorname{tr}\mathbf{E} = \ln J \tag{13}$$

denoting the volumetric part of the logarithmic elastic strain, Gearing and Anand [8] proposed the following modification to (11):

$$\psi(\mathbf{E}) = \mu_0 \, |\mathbf{E}_0|^2 + \kappa_0 (\epsilon_{\text{c}})^2 \left[1 - \left(1 + \frac{\epsilon}{\epsilon_{\text{c}}}\right) \exp\left(-\frac{\epsilon}{\epsilon_{\text{c}}}\right)\right], \tag{14}$$

where ϵ_{c} is a critical value of the elastic volumetric strain (a material parameter), and as before, μ_0 and κ_0 are the ground-state shear and bulk moduli of infinitesimal

isotropic elasticity. This three-constant free energy function was used by Gearing and Anand [8] to model the brittle cracking phenomenon observed experimentally in states of high triaxial tension in front of sharp notches in amorphous polymers. Also, see Henann and Anand [9] for an application of such a free energy function to model fracture of metallic glasses.

In writing (14), Gearing and Anand [8] assumed that $|\mathbf{E}_0|$ does not affect the volumetric part of the free energy. Correspondingly, they also assumed that the volumetric elastic strain ϵ does not affect the deviatoric part of the free energy. As pointed out by Veprek et al. [10], this lack of interaction between the deviatoric and volumetric parts of the free energy is not well-justified, especially at large volumetric strains. To remedy this situation, they proposed a free energy function of the form

$$\psi(\mathbf{E}) = \mu_0 \, \exp\left(-\frac{\epsilon}{\epsilon_c}\right) |\mathbf{E}_0|^2 + \kappa_0(\epsilon_c)^2 \left[1 - \left(1 + \frac{\epsilon}{\epsilon_c}\right) \exp\left(-\frac{\epsilon}{\epsilon_c}\right)\right]. \tag{15}$$

However, the coupling introduced in the first term of (15) by Veprek et al. [10] was based on an assumption that the classical Poisson's ratio (as defined at infinitesimal strains) remains *constant* even under large volumetric strains[2] — an assumption which is unsupported by either rigorous physical arguments or experimental observations. Indeed, estimates of the pressure sensitivity of the bulk modulus and the shear modulus from seismological studies shows that the Poisson's ratio increases with volumetric-compaction; cf., e.g., the discussion in Section 8 of Stacey and Davis [11].

Since it is difficult to conduct physical experiments to determine volumetric-deviatoric coupling effects under circumstances involving large volumetric strains, it is the purpose of this paper

- *to conduct numerical experiments — using molecular dynamics simulations — to explore such coupling effects in the free energy, and based on the results of these numerical experiments, to propose a simple continuum-level isotropic elastic free energy that captures the observed coupling effects.*

As we are concerned here with a free energy function for *isotropic materials*, in our molecular dynamics simulations we consider an *amorphous metallic glass* as our representative isotropic material.

The plan of this paper is as follows. In Section 2, we describe a simple free energy function specialized for large volumetric strains but small distortional strains. The results from our molecular dynamics simulations for various combinations of homogeneous volumetric and pure-shear deformations are described in Section 3. Based on the results of these numerical experiments, in Section 4 we construct a simple continuum-level isotropic elastic free energy that captures the volumetric-deviatoric coupling effects observed in our numerical experiments.

Plastic flow in metallic materials is known to be "pressure sensitive" — a sensitivity that cannot be ignored at high pressures; accordingly, in Section 5, we examine the effect of the volumetric strain on the effective shear stress required for the onset of plastic flow in the metallic glass, and correlate this dependence with the numerically-observed dependence of the elastic shear modulus on the volumetric strain. We close in Section 6 with some concluding remarks.

[2] Cf., the discussion in Section 2.2 of Veprek et al. [10].

2 A simple free energy function that couples the deviatoric and volumetric response

As before, let $\mathbf{E}$ denote the logarithmic strain, $\epsilon = \mathrm{tr}\,\mathbf{E}$ the volumetric part of the strain, and $|\mathbf{E}_0|$ the magnitude of the deviatoric part of $\mathbf{E}$. As indicated in (9), for isotropic materials the deviatoric strain $\mathbf{E}_0$ may contribute to the free energy through the second invariant $I_2 = \mathrm{tr}\,(\mathbf{E}_0^2)$ as well as the third invariant $I_3 = \mathrm{tr}\,\mathbf{E}_0^3$. However, *for small deviatoric strains* we expect that the effect of I_3, which is third-order in $\mathbf{E}_0$, is significantly smaller than the effect of I_2, which is second-order in $\mathbf{E}_0$. Accordingly,

- for small values of $|\mathbf{E}_0|$, which is of primary concern in this paper, we assume from the outset that the free energy does not depend upon the third invariant $I_3 = \mathrm{tr}\,(\mathbf{E}_0^3)$.

We provide a more detailed justification for this assumption in the Appendix.

Then, motivated by (15), we introduce two scalar valued functions $\mu(\epsilon)$ and $g(\epsilon)$, and consider a free energy function of the form

$$\psi(\mathbf{E}) = \mu(\epsilon)\,|\mathbf{E}_0|^2 + g(\epsilon). \tag{16}$$

Here $\mu(\epsilon)$ is a volumetric strain-dependent *generalized shear modulus*. We assume that

$$\mu(\epsilon) > 0 \tag{17}$$

for all values of ϵ considered in this paper, and denote the ground-state value of this generalized shear modulus by

$$\mu_0 \equiv \mu(0) > 0. \tag{18}$$

The term $g(\epsilon)$ in (16) represents a purely volumetric contribution to the free energy when $\mathbf{E}_0 = \mathbf{0}$. Let

$$\bar{\sigma}(\epsilon) \stackrel{\text{def}}{=} \frac{\mathrm{d}g(\epsilon)}{\mathrm{d}\epsilon} \tag{19}$$

denote a mean normal stress under this circumstance, and correspondingly define a *generalized bulk modulus* by

$$\kappa(\epsilon) \stackrel{\text{def}}{=} \frac{\mathrm{d}\bar{\sigma}(\epsilon)}{\mathrm{d}\epsilon} = \frac{\mathrm{d}^2 g(\epsilon)}{\mathrm{d}\epsilon^2}. \tag{20}$$

We limit our discussion in this paper to circumstances in which the generalized bulk modulus is positive-valued,

$$\kappa(\epsilon) > 0, \tag{21}$$

and denote the ground-state value of the generalized bulk modulus by

$$\kappa_0 \equiv \kappa(0) > 0. \tag{22}$$

Further, in order to ensure that the free energy at zero strain is zero-valued and that the reference configuration is stress-free, we require that

$$g(0) = 0 \qquad \text{and} \qquad \left.\frac{\mathrm{d}g(\epsilon)}{\mathrm{d}\epsilon}\right|_{\epsilon=0} = 0. \tag{23}$$

The Kirchhoff stress corresponding to the free energy (16) is then given by

$$\mathbf{T}_{\rm K} = \frac{\partial \psi(\mathbf{E})}{\partial \mathbf{E}} = 2\mu(\epsilon)\mathbf{E}_0 + \left(\bar{\sigma}(\epsilon) + \frac{\mathrm{d}\mu(\epsilon)}{\mathrm{d}\epsilon}\,|\mathbf{E}_0|^2\right)\mathbf{1}. \tag{24}$$

Next, let

$$\sigma \stackrel{\rm def}{=} \frac{1}{3}\mathrm{tr}\,\mathbf{T}_{\rm K}, \qquad \tau \stackrel{\rm def}{=} \frac{1}{\sqrt{2}}\,|\mathbf{T}_{{\rm K},0}|\,, \qquad \text{and} \qquad \gamma \stackrel{\rm def}{=} \sqrt{2}|\mathbf{E}_0| \tag{25}$$

define a *mean normal stress*, an *equivalent shear stress*, and an *equivalent shear strain*, respectively. Then (24) gives

$$\sigma = \hat{\sigma}(\epsilon,\gamma) = \bar{\sigma}(\epsilon) + \frac{1}{2}\frac{\mathrm{d}\mu(\epsilon)}{\mathrm{d}\epsilon}\gamma^2 \qquad \text{and} \qquad \tau = \hat{\tau}(\epsilon,\gamma) = \mu(\epsilon)\gamma. \tag{26}$$

Thus, note that the free energy function (16) gives a mean normal stress that depends not only on the volumetric strain but also on the equivalent shear strain γ: the term $\bar{\sigma}(\epsilon)$ in $(26)_1$ represents a mean normal stress versus volumetric strain response in the absence of a shear strain, while the term $\frac{1}{2}(\mathrm{d}\mu(\epsilon)/\mathrm{d}\epsilon)\gamma^2$ represents a *shear-induced mean normal stress*. Also, the equivalent shear stress τ depends not only on the equivalent shear strain but also on the volumetric strain ϵ, with $\mu(\epsilon)$ in $(26)_2$ representing a volumetric strain-dependent generalized shear modulus,

In the next section, we report on our numerical experiments using molecular dynamics simulations on a metallic glass. We shall use the stress-strain results from these numerical experiments to fit specific forms for the functions $g(\epsilon)$ and $\mu(\epsilon)$.

3 Molecular dynamics simulations

Since we are concerned with a free energy function for isotropic materials, in our molecular dynamics simulations, we consider an amorphous metallic glass as our representative isotropic material. Also, in order to determine specific forms for the functions $\mu(\epsilon)$ and $g(\epsilon)$ in the free energy (16), we take a pragmatic mechanics-based approach, treating the results from molecular dynamics simulations as we would results from physical experiments, and determine $g(\epsilon)$ and $\mu(\epsilon)$ by selecting specific forms which fit our "experimental" data in the range of volumetric and shear strain levels for which we have conducted our numerical simulations.[3]

3.1 Preparation of a metallic glass specimen

Following Cao et al. [13] and Cheng et al. [14], we consider a metallic glass with a composition of $Cu_{64}Zr_{36}$ and use the embedded atom potential developed and validated (using density functional theory calculations) for this system by these authors. To prepare a metallic glass specimen, we use a three-dimensional box of 10,976 atoms under periodic boundary conditions in all three dimensions. The sample was first equilibrated for 2 ns at 2000 K and zero external pressure to ensure

[3] For details on the theory and practice of molecular dynamics simulations, see the text by Frenkel and Smit [12].

melting and then quenched at a rate of 100 K/ns to a temperature of 50 K at zero external pressure using a Nose-Hoover thermostat and the NPT ensemble. Figures 1(a) and (b), respectively, show the specific volume and specific enthalpy as a function of temperature during quenching. The markers represent the average of each quantity over temperature spans of 50 K.[4] Figure 2 shows the radial distribution functions for Cu-Cu, Cu-Zr, and Zr-Zr pairs, confirming that the as-quenched sample is *amorphous*. From the data in Figs. 1(a) and (b), the glass transition temperature $\vartheta_{\rm g}$, the volumetric coefficient of thermal expansion β below $\vartheta_{\rm g}$, and the specific heat at constant pressure $c_{\rm p}$ below $\vartheta_{\rm g}$ for the simulated amorphous alloy were determined to be

$$\vartheta_{\rm g} = 664\,K, \quad \beta = 33.6 \times 10^{-6}\,{\rm K}^{-1}, \quad \text{and} \quad c_{\rm p} = 0.19\,\frac{\rm J}{\rm kg\,K}, \tag{27}$$

respectively.

A schematic of the as-quenched configuration, which we will refer to as the reference configuration of the body B, is shown in Fig. 3, which also shows a snapshot of the molecular configuration of the sample; the copper atoms are copper-colored and the zirconium atoms are white. The sample after quenching has dimensions of 5.62 nm in the 1, 2, and 3-directions.

3.2 Numerical experiments on the metallic glass specimen

The $Cu_{64}Zr_{36}$ metallic glass sample was subjected to various combinations of volumetric and shear strain, under periodic boundary conditions and a constant temperature of 50 K, using the NVT ensemble. The various deformations considered are summarized below:

1. **Volumetric dilatation/compaction**: The sample is subjected to purely volumetric deformation with equal principal stretches:

   $$\lambda_1 = \lambda_2 = \lambda_3 = \lambda.$$

   A schematic of the deformed body $\mathcal{B}_t$ for such a deformation is shown in Fig. 4(a);[5] this figure also shows a corresponding snapshot of the molecular configuration at a volumetric strain of $\epsilon = 0.15$.
2. **Pure shear**: The sample is subjected to volume-conserving pure shear:

   $$\lambda_1 = \lambda, \qquad \lambda_2 = 1/\lambda, \qquad \text{and} \qquad \lambda_3 = 1.$$

   A schematic of the deformed body $\mathcal{B}_t$ for such a deformation is shown in Fig. 4(b); this figure also shows a corresponding snapshot of the MD configuration at a shear strain of $\gamma = 0.04$.
   - *For sufficiently large shear strains, the metallic glass sample will deform plastically; however, in this numerical experiment, and in all other experiments involving shear strains that follow (except those discussed in Section 5), we limit the magnitude of shear strain so that the sample remains in the elastic range.*

[4] The error bars in these figures denote the maximum and minimum values of each quantity measured over temperature spans of 50 K during the quenching simulations.

[5] The magnitude of strain in the schematics shown in Fig. 4 is exaggerated for ease of visualization.

3. **Volumetric deformation followed by pure shear**: The sample is first subjected to various levels of volumetric dilatation and compaction, and then subjected to pure shear.
4. **Pure shear followed by volumetric deformation**: The sample is first subjected to various levels of shear strain, and then subjected to volumetric dilatation and compaction.

The stress-strain results from each of these numerical experiments are discussed below.

3.3 Volumetric dilatation/compaction

The sample was subjected to a constant volumetric strain rate of $\dot{\epsilon} = \pm 3\times 10^8\,\mathrm{s}^{-1}$ in dilatation/compaction. The components of the Cauchy stress may be determined from the virial stress. However, since our stress-strain relation (24) is given in terms of the Kirchhoff stress ($\mathbf{T}_{\mathrm{K}} = J\mathbf{T}$), in what follows, unless otherwise specified, *we report all stress-related quantities in terms of the Kirchhoff stress.*

Figure 5 shows the mean normal stress σ as a function of the volumetric strain ϵ, for ϵ in the range $[-0.30, 0.15]$. The corresponding range of mean normal stress σ is approximately $[-45, 15]\,\mathrm{GPa}$ — the dependence of σ on ϵ in this large range of volumetric strains is clearly *nonlinear*.

It is important to note that at sufficiently large compressive volumetric strains the numerical metallic glass specimen exhibits *ordering*, while at sufficiently large positive volumetric strains the specimen exhibits *cavitation-induced* fracturing. Figure 6(a) shows the radial distribution functions for Zr-Zr pairs in the quenched state, and at a volumetric strain of $\epsilon = -0.35$, where evidence of strain-induced ordering can be observed; and Fig. 6(b) shows a snapshot of a slice of the molecular configuration at a volumetric strain of $\epsilon \approx 0.16$, where cavitation-related failure is evident. By examining the radial distribution functions for Cu-Cu, Cu-Zr, and Zr-Zr pairs for volumetric strains in the range $[-0.30, 0]$, we have confirmed that no strain-induced ordering occurs in our simulations; correspondingly for volumetric strains in the range $[0, 0.15]$, we do not observe any cavitation-related failure. *Thus, for ϵ in the range $[-0.30, 0.15]$ studied in this paper, the metallic glass specimen used in our numerical experiments continues to respond as an intact, nominally-isotropic, amorphous material.*

3.4 Pure shear

The sample was subjected to volume-conserving pure shear at a shear strain rate of $\dot{\gamma} = 1 \times 10^8\,\mathrm{s}^{-1}$ to a final shear strain of $\gamma = 0.04$.[6] The resulting shear stress τ versus shear strain γ is plotted in Fig. 7(a). The dependence of τ on γ in this range of shear strains is essentially linear.

Interestingly, the plot in Fig. 7(b) shows that *a small but non-negligible non-zero mean normal stress develops during pure shear.* More on this later.

[6] The strain was reversed to verify that no appreciable permanent deformation had occurred at this level of shear strain.

3.5 Volumetric deformation followed by pure shear

The sample was first subjected to volumetric strains ranging from $\epsilon = -0.15$ to $\epsilon = 0.15$, and subsequently subjected to reversed volume-conserving pure shear to a final shear strain of $\gamma = 0.02$. For clarity, in Fig. 8(a) we only show the shear stress τ versus shear strain γ for volumetric strains of $\epsilon = -0.09, 0, 0.09$.

Figure 8(b) shows the shear modulus μ as a function of the volumetric strain ϵ, and from this figure it is evident that *the shear modulus decreases with volumetric dilatation and increases with volumetric compaction.*

3.6 Pure shear followed by volumetric deformation

The sample was first subjected to pure shear to strains of $\gamma = 0.02, 0.04$, then subjected to volumetric strains ranging from $\epsilon = -0.15$ to $\epsilon = 0.15$. The mean normal stress σ is plotted against the volumetric strain ϵ in Fig. 9(a) for the different values of prior shear strain. From this figure it is clear that *a prior shear strain, in the limited range of accessible elastic shear strains, has a negligible effect on the subsequent volumetric stress-strain response.*

Figure 9(c) shows the variation of the shear stress τ as a function of the volumetric strain ϵ for the two different levels of prior shear strains, $\gamma = 0.02, 0.04$. This figure clearly shows that *the shear stress generated by a prior shear strain is significantly affected by a subsequent volumetric deformation.*

4 Specialization of the functions $g(\epsilon)$ and $\mu(\epsilon)$

In this section, we use the stress-strain results from our molecular dynamics simulations to select and calibrate specialized forms for the functions $g(\epsilon)$ and $\mu(\epsilon)$. We emphasize from the outset that our focus is on motivating proper functional forms rather than the specific values of the parameters appearing in the specialized functions. The actual values of the material parameters will of course be valid only for this *numerical* $Cu_{64}Zr_{36}$ metallic glass, and are controlled by its underlying interatomic potential.

4.1 Determination of the function $g(\epsilon)$

Recall from (19) and (20) that the mean normal stress in the absence of a shear strain and the generalized bulk modulus are defined in terms the function $g(\epsilon)$ by

$$\bar{\sigma}(\epsilon) \stackrel{\text{def}}{=} \frac{\mathrm{d}g(\epsilon)}{\mathrm{d}\epsilon} \qquad \text{and} \qquad \kappa(\epsilon) \stackrel{\text{def}}{=} \frac{\mathrm{d}^2 g(\epsilon)}{\mathrm{d}\epsilon^2}. \tag{28}$$

Following Gearing and Anand [8], we adopt[7]

$$g(\epsilon) = \kappa_0(\epsilon_c)^2 \left[1 - \left(1 + \frac{\epsilon}{\epsilon_c}\right) \exp\left(-\frac{\epsilon}{\epsilon_c}\right)\right], \tag{29}$$

[7] This form is motivated by the *universal binding energy relation* (UBER) for a one-dimensional interatomic potential introduced by Rose et al. [7].

where κ_0 is the ground-state bulk modulus, and $\epsilon_c > 0$ is another material constant representing a critical value of the elastic volumetric strain associated with *cavitation* in volumetric dilatation. Applying the relations (28) gives

$$\begin{aligned} \bar{\sigma}(\epsilon) &= \left[\kappa_0 \exp\left(-\frac{\epsilon}{\epsilon_c}\right)\right]\epsilon, \\ \kappa(\epsilon) &= \kappa_0 \left(1 - \frac{\epsilon}{\epsilon_c}\right) \exp\left(-\frac{\epsilon}{\epsilon_c}\right). \end{aligned} \tag{30}$$

Fitting the function $(30)_1$ to the results of our molecular dynamics simulations shown in Fig. 5(a), gives

$$\kappa_0 = 120.0\,\text{GPa} \quad \text{and} \quad \epsilon_c = 1.0. \tag{31}$$

The quality of the fit for the mean normal stress versus volumetric strain response using these material parameters is shown in Fig. 5.

Remark: Since the generalized bulk modulus $\kappa(\epsilon)$ in $(30)_2$ reaches zero at ϵ_c and becomes negative for $\epsilon > \epsilon_c$, an instability will occur at $\epsilon = \epsilon_c$. Softening hyperelasticity models of this type have been used to model cavitation failure in a variety of materials (cf., e.g., [8,9]). However, we do not focus on cavitation phenomena or the prediction of cavitation here (cf., Fig. 6 b), because it is our belief that cavitation is initiated at heterogeneities in the microstructure which are not explicitly included in our molecular dynamics simulations.

4.2 Determination of the function $\mu(\epsilon)$

We determine the form of the generalized shear modulus function $\mu(\epsilon)$ by fitting the simulation results of volumetric deformation followed by pure shear, cf. Fig. 8(b). To this end, we choose a fitting function of the form

$$\mu(\epsilon) = \mu_r - (\mu_r - \mu_0) \exp\left(\frac{\epsilon}{\epsilon_r}\right), \tag{32}$$

where μ_0 is the ground state shear modulus at $\epsilon = 0$, μ_r is the value of the generalized shear modulus that is asymptotically approached as $\epsilon \to -\infty$, and ϵ_r is a reference value of the volumetric strain. Fitting the function (32) to the data of Fig. 8(b) we obtain

$$\mu_0 = 25.2\,\text{GPa}, \quad \mu_r = 29.7\,\text{GPa} \quad \text{and} \quad \epsilon_r = 0.12. \tag{33}$$

The quality of the fit for the shear stress versus shear strain response, and the generalized shear modulus versus volumetric strain using these material parameters, is shown in Figs. 8(a) and 8(b), respectively.

Remark: The material parameter μ_0 represents the ground-state shear modulus. We do not attribute any fundamental physical significance to the two additional material parameters (μ_r, ϵ_r); they are phenomenological constants that fit our numerically-generated data over the range of volumetric strains ϵ studied here. In particular, note that ϵ_r appearing in the expression (32) for the generalized shear modulus is not related to ϵ_c appearing in the expression $(30)_2$ for the generalized bulk modulus.

4.3 Partial validation of the coupled free energy function

Next we perform a partial validation of the coupled free energy function (16) with $g(\epsilon)$ and $\mu(\epsilon)$ given in (29) and (32). To do this we revisit the results from our numerical simulations for pure shear, and pure shear followed by volumetric deformation.

First, we note that in the case of pure shear at $\epsilon = 0$, (26) and (32) predict the following shear-induced mean stress

$$\sigma = \frac{1}{2}\left.\frac{\mathrm{d}\mu(\epsilon)}{\mathrm{d}\epsilon}\right|_{\epsilon=0}\gamma^2 = -\frac{1}{2}\frac{(\mu_\mathrm{r}-\mu_0)}{\epsilon_\mathrm{r}}\gamma^2. \tag{34}$$

Using the parameter list (33), the predicted shear-induced mean normal stress is compared to the result from the molecular dynamics simulation in Fig. 7(b), and the comparison is quite good. Thus,

- *the shear-induced mean stress predicted by the molecular dynamics simulations, which at first blush seems unphysical, is a direct outcome of the volumetric strain-dependent shear modulus function $\mu(\epsilon)$.*

Next, we compare the prediction of our hyperelasticity model with the molecular dynamics results for the case of pure shear followed by volumetric deformation. Using (26) in conjunction with $(30)_1$ and (32), our model predicts

$$\begin{aligned}
\sigma &= \hat{\sigma}(\epsilon,\gamma) = \left[\kappa_0 \exp\left(-\frac{\epsilon}{\epsilon_\mathrm{c}}\right)\right]\epsilon - \frac{1}{2}\frac{(\mu_\mathrm{r}-\mu_0)}{\epsilon_\mathrm{r}}\exp\left(\frac{\epsilon}{\epsilon_\mathrm{r}}\right)\gamma^2,\\
\tau &= \hat{\tau}(\epsilon,\gamma) = \left[\mu_\mathrm{r} - (\mu_\mathrm{r}-\mu_0)\exp\left(\frac{\epsilon}{\epsilon_\mathrm{r}}\right)\right]\gamma,
\end{aligned} \tag{35}$$

for the mean normal stress and the equivalent shear stress, respectively. The predictions from these equations, using the parameter lists (31) and (33), are compared to the molecular dynamics simulation results in Fig. 9. Figure 9(b) shows that the predicted mean stress versus volumetric strain response matches that which is observed in the molecular dynamics simulations. Note that since the final term in $(35)_1$ is second order in the shear strain γ, it has an indiscernible effect on the mean normal stress versus volumetric strain response for the range of shear strains considered here. In contrast, for fixed γ, the variation of the shear modulus with volumetric strain has a marked effect on the variation of the shear stress with the volumetric strain. Figure 9(c) shows that the predictions from $(35)_2$ reasonably match the results from the molecular dynamics simulation.

5 Pressure-dependence of the plastic flow strength

In the literature on plastic flow of metals under extreme conditions of pressure and strain rate (cf., e.g., Remington et al. [15] for a recent review), the plastic flow strength in shear (under isothermal conditions), S, is often taken to be given by

$$S = f(\bar{\gamma}^p, \dot{\bar{\gamma}}^p)\,\frac{\mu(P)}{\mu_0}, \tag{36}$$

where $f(\bar{\gamma}^p, \dot{\bar{\gamma}}^p)$ is a function of the equivalent plastic shear strain $\bar{\gamma}^p$ and the equivalent plastic shear strain rate $\dot{\bar{\gamma}}^p$, and the flow strength S is presumed to

scale with the ratio $\mu(P)/\mu_0$, where $\mu(P)$ is the pressure-dependent elastic shear modulus and μ_0 is the value of the elastic shear modulus at zero pressure. Instead of taking the shear modulus μ to be a function of the pressure P, *for our purposes* it is more useful to take μ to be a function of the elastic volumetric strain

$$\epsilon^e \stackrel{\text{def}}{=} \operatorname{tr} \mathbf{E}^e,$$

with $\mathbf{E}^e$ the logarithmic elastic strain in a theory for elastic-plastic deformation of metals,[8] and alternatively write (36) as

$$S = f(\gamma^p, \dot{\bar{\gamma}}^p)\, \frac{\mu(\epsilon^e)}{\mu_0}. \tag{37}$$

In this section, we explore the correlation between the volumetric strain-dependence of the shear modulus from Section 4.2 and that of the plastic flow strength (37).

In order to determine the plastic flow strength at different levels of elastic volumetric strain, we carried out molecular dynamics simulations in which the sample is first subjected to a prescribed volumetric strain, and then subjected to increasing pure shear strain until plastic deformation ensues. Figure 10(a) shows the shear stress versus shear strain response up to a shear strain of $\gamma = 0.15$ at three different elastic volumetric pre-strains, $\epsilon^e = -0.09, 0, 0.09$. In all three cases, a nominally linear elastic response is observed up to a shear strain of $\gamma \approx 0.06 - 0.08$, at which point inelastic deformation sets in. The stress-strain results from the molecular dynamics simulations are quite noisy, and the level of the shear stress in the inelastic region shows significant fluctuations; accordingly, we average the stress over the range of shear strains $\gamma \in [0.08, 0.12]$ and take this average as the value of plastic flow strength at $\bar{\gamma}^p \approx 0$ and a high molecular dynamics strain rate of $\dot{\bar{\gamma}}^p = 1 \times 10^8\, \mathrm{s}^{-1}$, denoting it by S_0. Such averaged plastic flow strength values S_0 are plotted as a function of the prior volumetric elastic strain ϵ^e in Fig. 10(b).[9] Using (37) and (32), the elastic volumetric strain dependence of S_0 is predicted to be

$$S_0 = f_0 \left[\frac{\mu_{\mathrm{r}}}{\mu_0} - \left(\frac{\mu_{\mathrm{r}}}{\mu_0} - 1 \right) \exp\left(\frac{\epsilon^e}{\epsilon_{\mathrm{r}}} \right) \right]. \tag{38}$$

The prediction of the variation of S_0 with ϵ^e, using the parameter list (33), is also plotted in Fig. 10(b). The agreement from the model (38) with the results of the numerical simulations is quite good. This good agreement strongly indicates that one contribution to the "pressure-dependence" of plastic flow in metallic glasses is directly related to the "elastic volumetric strain-dependence" of the shear modulus of the material. Our numerical simulation results also support the scaling relation (36) (or equivalently (37)) for the "pressure-sensitivity" of plastic flow used in the metal physics community.

[8] Here we have in mind an isotropic theory of elastic-plastic solids based on the multiplicative decomposition of the deformation gradient $\mathbf{F} = \mathbf{F}^e\mathbf{F}^p$, in which $\mathbf{F}^e$ and $\mathbf{F}^p$ are elastic and plastic distortions, respectively, and where $\mathbf{E}^e = \ln \mathbf{V}^e$, with $\mathbf{V}^e$ the left elastic stretch tensor in the polar decompostion $\mathbf{F}^e = \mathbf{V}^e\mathbf{R}^e$.

[9] The error bars in this figure denote the maximum and minimum values of shear stress encountered in defining the onset of plastic flow in our numerical simulations.

6 Concluding remarks

The Hencky [2–4]-Anand [5,6] free energy and stress-strain relation for moderately large elastic strains are given by

$$\begin{aligned}\psi(\mathbf{E}) &= \mu_0|\mathbf{E}_0|^2 + \frac{1}{2}\kappa_0(\mathrm{tr}\,\mathbf{E})^2,\\ \mathbf{T}_{\mathrm{K}} &= 2\mu_0\mathbf{E}_0 + \kappa_0(\mathrm{tr}\,\mathbf{E})\mathbf{1},\end{aligned} \tag{39}$$

with $\mu_0 > 0$ and $\kappa_0 > 0$ the classical shear and bulk moduli from the infinitesimal theory of elasticity.

Based on molecular dynamics simulations of a metallic glass, we have attempted to extend the range of applicability of the Hencky-Anand theory to situations involving large volumetric strains, and have proposed the following free energy function

$$\begin{aligned}&\psi(\mathbf{E}) = \mu(\mathrm{tr}\,\mathbf{E})\,|\mathbf{E}_0|^2 + g(\mathrm{tr}\,\mathbf{E}), \qquad \text{with}\\ &\mu(\mathrm{tr}\,\mathbf{E}) = \mu_{\mathrm{r}} - (\mu_{\mathrm{r}} - \mu_0)\exp\left(\frac{\mathrm{tr}\,\mathbf{E}}{\epsilon_{\mathrm{r}}}\right), \qquad \text{and}\\ &g(\mathrm{tr}\,\mathbf{E}) = \kappa_0(\epsilon_{\mathrm{c}})^2\left[1 - \left(1 + \frac{\mathrm{tr}\,\mathbf{E}}{\epsilon_{\mathrm{c}}}\right)\exp\left(-\frac{\mathrm{tr}\,\mathbf{E}}{\epsilon_{\mathrm{c}}}\right)\right].\end{aligned} \tag{40}$$

The Kirchhoff stress corresponding to the free energy (40) is given by

$$\begin{aligned}\mathbf{T}_{\mathrm{K}} =& 2\left[\mu_{\mathrm{r}} - (\mu_{\mathrm{r}} - \mu_0)\exp\left(\frac{\mathrm{tr}\,\mathbf{E}}{\epsilon_{\mathrm{r}}}\right)\right]\mathbf{E}_0\\ &+ \left\{\left[\kappa_0\exp\left(-\frac{\mathrm{tr}\,\mathbf{E}}{\epsilon_{\mathrm{c}}}\right)\right]\mathrm{tr}\,\mathbf{E} - \left[\frac{(\mu_{\mathrm{r}} - \mu_0)}{\epsilon_{\mathrm{r}}}\exp\left(\frac{\mathrm{tr}\,\mathbf{E}}{\epsilon_{\mathrm{r}}}\right)\right]|\mathbf{E}_0|^2\right\}\mathbf{1}.\end{aligned} \tag{41}$$

The new free energy and corresponding stress-strain relation have five material constants — the two classical positive-valued shear and bulk moduli μ_0 and κ_0 of the infinitesimal theory of elasticity, and three additional positive-valued material constants $(\mu_{\mathrm{r}}, \epsilon_{\mathrm{r}}, \epsilon_{\mathrm{c}})$, which are used to characterize the nonlinear response at large values of $\mathrm{tr}\,\mathbf{E}$. In the large volumetric strain range $-0.30 \leq \mathrm{tr}\,\mathbf{E} \leq 0.15$ but small shear strain range $\sqrt{2}|\mathbf{E}_0| \lessapprox 0.05$ numerically explored in this paper, this simple five-constant model provides a very good description of the stress-strain results from our molecular dynamics simulations.

As reviewed by Veprek et al. [10], recently-developed coating materials possess ultra-high hardness in the range of 40–100 GPa. The mechanical properties of these thin coating materials are primarily assessed by means of load-versus-depth sensing indentation techniques. During indentation tests on hard materials, a very high pressure builds up in the sample under the indenter, and this causes the elastic moduli and plastic flow strength to increase substantially. It is of central importance to account for such nonlinear behavior when simulating indentation experiments, or using experimental data from indentation experiments to infer hardness and other mechanical properties of ultra-hard materials. Our new free energy function (40) and the attendant stress-strain relation (41) should be useful in analyzing the results of load-depth indentation experiments on ultra-hard materials.

In the absence of deviatoric strains, our theory produces a pressure-volume equation-of-state (EOS) which extends a relation based on the logarithmic strain

measure proposed by Poirier and Tarantola [16]. As reviewed by Stacey and Davis [11], the Poirier-Tarantola EOS is of substantial utility in describing the pressure-volume relationship in the *lower mantle* of the earth and is much better than the widely-used Birch [17] EOS. In addition to extending the range of applicability of the Poirier-Tarantola EOS to larger compressive volumetric strains, our more general theory explicitly accounts for the volumetric strain dependence of the generalized shear modulus $\mu(\mathrm{tr}\,\mathbf{E})$ — a coupling-effect which is of substantial importance in the geophysics literature on the high-pressure response of geological materials (cf., e.g., Stacey and Davis [11]).

Appendix

At the beginning of Section 2 we had argued that for small deviatoric strains we expected that the contribution to the free energy from $I_3 = \mathrm{tr}\,\mathbf{E}_0^3$ (which is third-order in $\mathbf{E}_0$) is significantly smaller than the effect of $I_2 = \mathrm{tr}\,\mathbf{E}_0^2$ (which is second-order in $\mathbf{E}_0$), and accordingly we had neglected any dependence of the free energy on I_3. In this Appendix we conduct numerical experiments in which I_3 is non-zero, and explore the effects of I_3 on the stress-strain response for circumstances under which $|\mathbf{E}_0|$ is small and limited to values for which $\gamma = \sqrt{2}|\mathbf{E}_0| \leq 0.04$, so that the sample remains in the elastic range. Specifically, to explore the effects of I_3 we consider,

- **Isochoric extension and isochoric compression**: In these two deformations the sample is subjected to volume-conserving deformation in which the principal stretches are given by

$$\lambda_1 = 1/\sqrt{\lambda}, \quad \lambda_2 = \lambda, \quad \text{and} \quad \lambda_3 = 1/\sqrt{\lambda}, \tag{42}$$

  with $\lambda > 1$ corresponding to isochoric extension, and $\lambda < 1$ corresponding to isochoric compression. A schematic of the deformed body $\mathcal{B}_t$ for isochoric extension is shown in Fig. 11(a), while that for isochoric compression is shown in Fig. 11(b).

In this case,

$$I_3 = \mathrm{tr}\,\mathbf{E}_0^3 = \pm\,\frac{3}{4}|\ln\lambda|^3, \tag{43}$$

with I_3 positive in tension and negative in compression.[10] Since we are restricting our attention to circumstances in which

$$\gamma = \sqrt{2}|\mathbf{E}_0| = \sqrt{3}|\ln\lambda| \leq 0.04,$$

we have $|\ln\lambda| \leq 0.04/\sqrt{3}$, which when substituted in (43) gives that I_3 lies in the range $[-9.24\times10^{-6}, 9.24\times10^{6}]$ for the isochoric extension and compression experiments under consideration here.

The molecular dynamics reference body, Figure 3, was subjected to isochoric extension and compression at an axial strain rate of $\pm1\times10^{8}\,\mathrm{s}^{-1}$ to a final shear strain of $\gamma = 0.04$. The resulting equivalent shear stress τ versus equivalent shear strain γ curves are plotted in Fig. 12(a). The dependence of τ on γ in this range

[10] Recall that in the case of pure shear considered earlier, $I_3 = 0$.

of shear strains for both isochoric extension and compression is *essentially linear and identical to each other*, as well as identical to the response in pure shear, cf. Fig. 7(a), in which $I_3 = 0$. Also shown Fig. 12(a) as a dotted line is the prediction of our calibrated hyperelasticity model, which ignores any dependence of I_3. Additionally, Fig. 12(b) shows the (small) non-zero mean normal stress that develops during isochoric extension and compression — again the results from the two MD simulations overlap each other, and correspond well to that predicted by (34) for the calibrated hyperelasticity model which ignores any dependence of I_3. Thus, we have demonstrated that

- for the small deviatoric strains $\gamma \leq 0.04$, the third invariant I_3 has no discernible effect on the stress-strain response, and our assumption that the free energy function (16) does not depend upon I_3 is well-justified.

Acknowledgements This paper is dedicated to the memory of Professor Donald E. Carlson, whose foundational work on the derivatives of a general class of strain measures [18] has enabled a wider use of the logarithmic strain measure in elasticity. Financial support was provided by grants from NSF (CMS-0555614) and the Singapore-MIT Alliance (MST).

References

1. Gurtin, M.E., Fried, E., Anand, L.: The Mechanics and Thermodynamics of Continua. Cambridge University Press, New York (2010)
2. Hencky, H.: Über die form des elastizitätsgesetzes bei ideal elastischen stoffen. Z. Techn. Phys. 9, 215–223 (1928)
3. Hencky, H.: The law of elasticity for isotropic and quasi-isotropic substances by finite deformations. J. Rheol. 2, 169–176 (1931)
4. Hencky, H.: The elastic behavior of vulcanised rubber. Rubber Chem. Technol. 6, 217–224 (1933)
5. Anand, L.: On H. Hencky's Approximate Strain-Energy Function for Moderate Deformations. J. Appl. Mech. 46, 78–82 (1979)
6. Anand, L.: Moderate deformations in extension-torsion of incompressible isotropic elastic materials. J. Mech. Phys. Solids 34, 293–304 (1986)
7. Rose, J.H., Smith, J.R., Ferrante, J.: Universal features of bonding in metals. Phys. Rev. B 28, 1835–1845 (1983)
8. Gearing, B.P., Anand, L.: Notch-sensitive fracture of polycarbonate. Int. J. Solids Struct. 41, 827–845 (2004)
9. Henann, D.L., Anand, L.: Fracture of metallic glasses at notches: effects of notch-root radius and the ratio of the elastic shear modulus to the bulk modulus on toughness. Acta Mater. 57, 6057–6074 (2009)
10. Veprek, R.G., Parks, D.M., Argon, A.S., Veprek, S.: Erratum to Non-linear finite element constitutive modeling of mechnical properties of hard and superhard materials studied by indentation. Mater. Sci. Eng. A 448, 366–378 (2007)
11. Stacey, F. D., Davis, P. M.: High pressure equations of state with applications to the lower mantle and core. Phys. Earth Planet. In. 142, 137–184 (2004)
12. Frenkel, D., Smit, B.: Understanding Molecular Simulation, Second Edition: From Algorithms to Applications. Academic Press, Boston (2002)
13. Cao, A.J., Cheng, Y.Q., Ma, E.: Structural processes that initiate shear localization in metallic glass. Acta Mater. 57, 5146-5155 (2009)
14. Cheng, Y.Q., Sheng, H.W., Ma, E.: Atomic level structure in multicomponent bulk metallic glass. Phys. Rev. Lett. 102, 245501 (2009)
15. Remington, B.A., Allen, P., Bringa, E.M., Hawreliak, J., Ho, D., Lorenz, K.T., Lorenzana, H., McNaney, J.M., Meyers, M.A., Pollaine, S.W., Rosolankova, K., Sadik, B., Schneider, M.S., Swift, D., Wark, J., Yaakobi, B.: Material dynamics under extreme conditions of pressure and strain rate. Mater. Sci. Tech. 22, 474-488 (2006)

16. Poirier, J.-P., Tarantola, A.: A logarithmic equation of state. Phys. Earth Planet. In. 109, 1–8 (1998)
17. Birch, F.: Elasticity and Constitution of the Earth Interior. J. Geophys. Res. 57 227–286 (1952)
18. Carlson, D.E., Hoger, A.: The derivative of a tensor-valued function of a tensor. Q. Appl. Math. 44, 409–423 (1986)

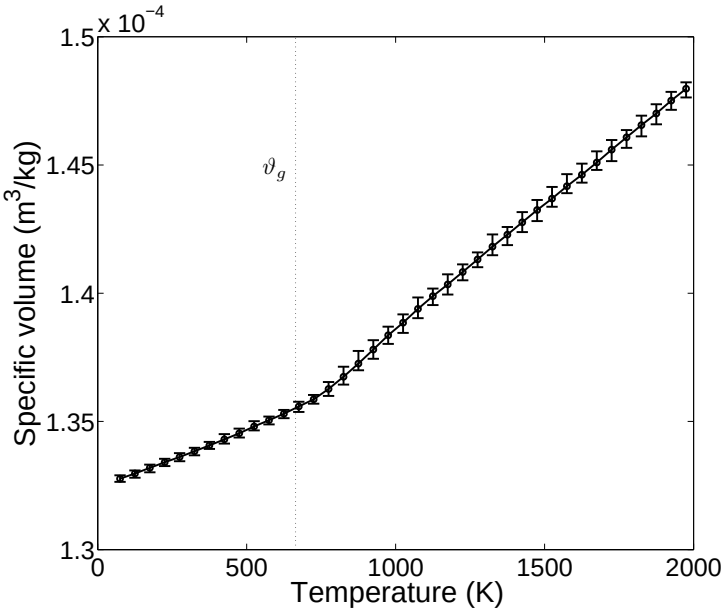

(a)

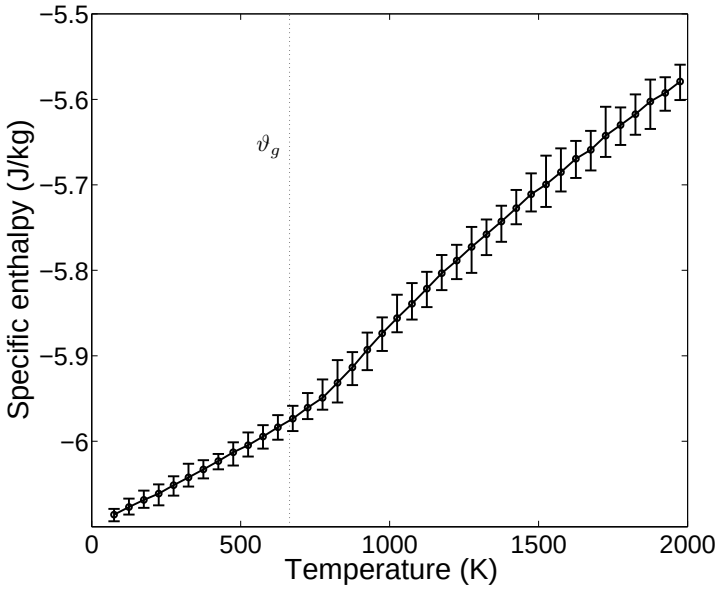

(b)

Fig. 1 (a) Specific volume and (b) specific enthalpy versus temperature.

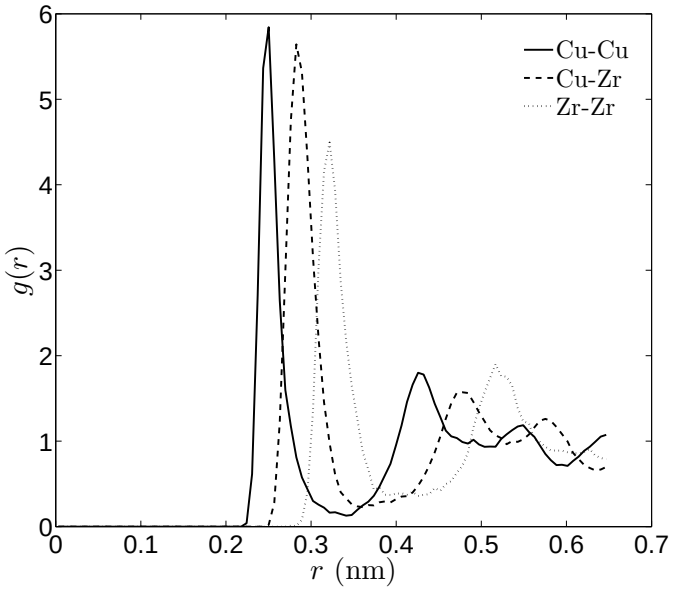

Fig. 2 The radial distribution functions in the quenched state for Cu-Cu, Cu-Zr, and Zr-Zr pairs, confirming the amorphous structure of the as-quenched sample.

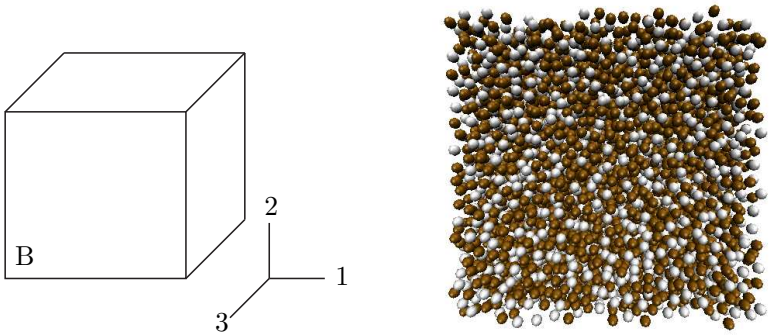

Fig. 3 Schematic and snapshot of the undeformed configuration.

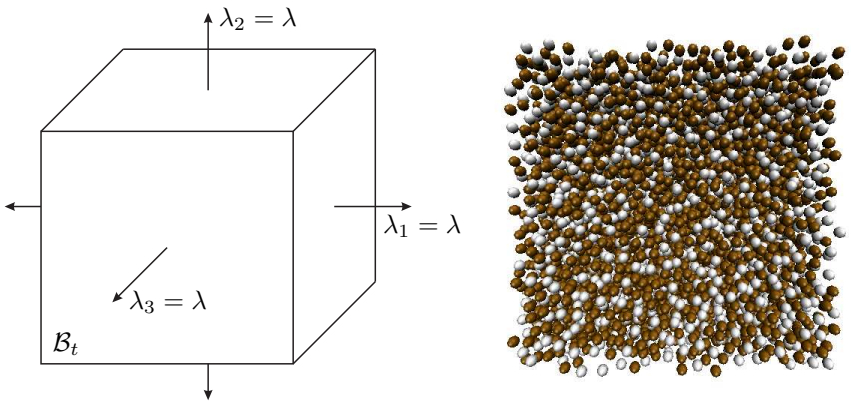

(a)

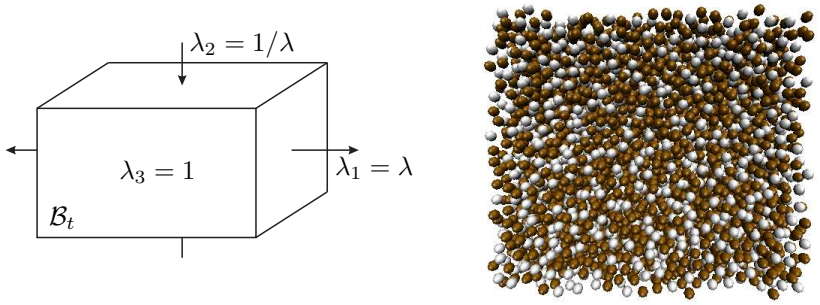

(b)

Fig. 4 Schematic and snapshots of the (a) dilated and (b) sheared configurations.

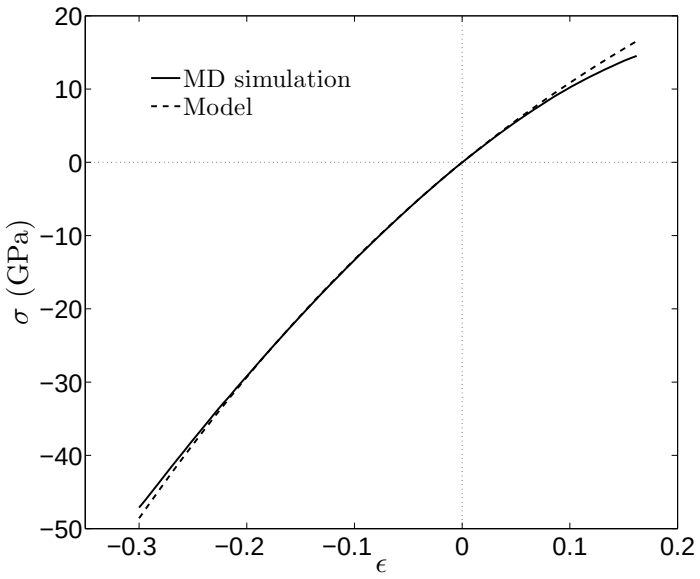

Fig. 5 Variation of the mean stress with elastic volumetric strain. The solid line is the result of the MD simulation, and the dashed line is the result of the calibrated hyperelasticity model.

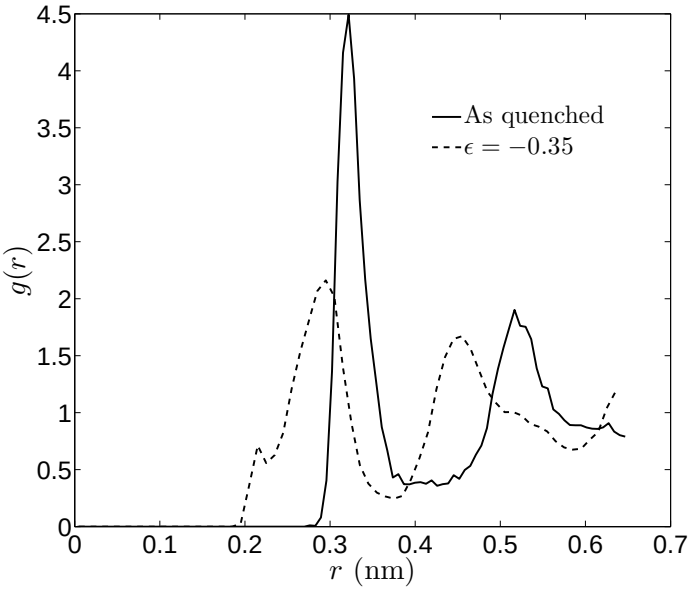

(a)

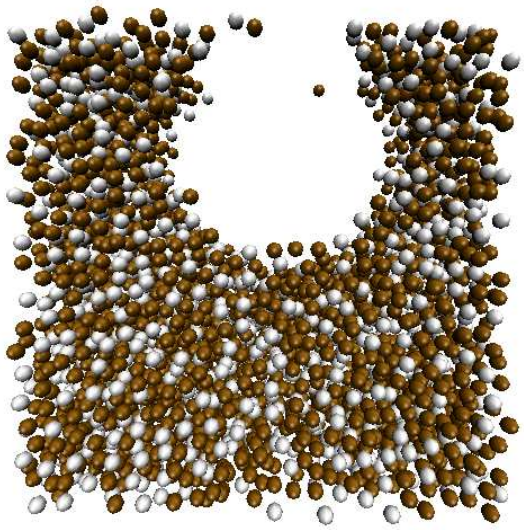

(b)

Fig. 6 (a) The radial distribution functions for Zr-Zr pairs in the quenched state and at a volumetric strain of $\epsilon = -0.35$, showing evidence of strain-induced ordering at high compressive volumetric strains. (b) A snapshot of a slice of the molecular specimen at a volumetric strain of $\epsilon \approx 0.16$, demonstrating cavitation-related failure.

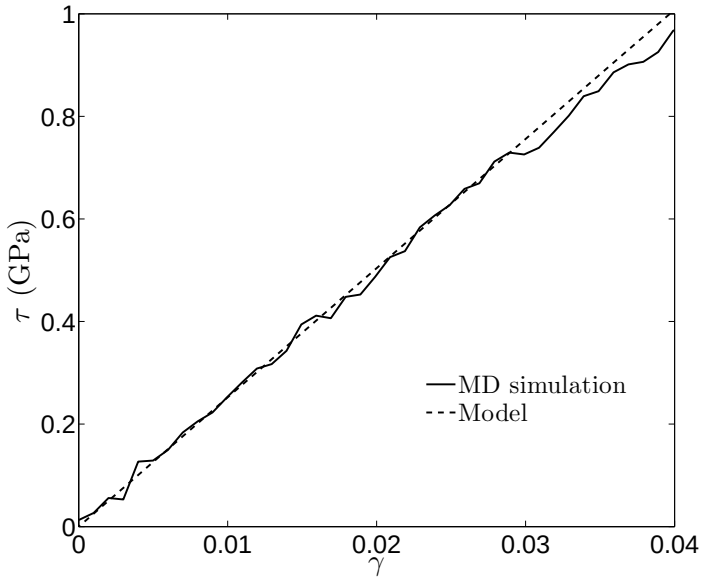

(a)

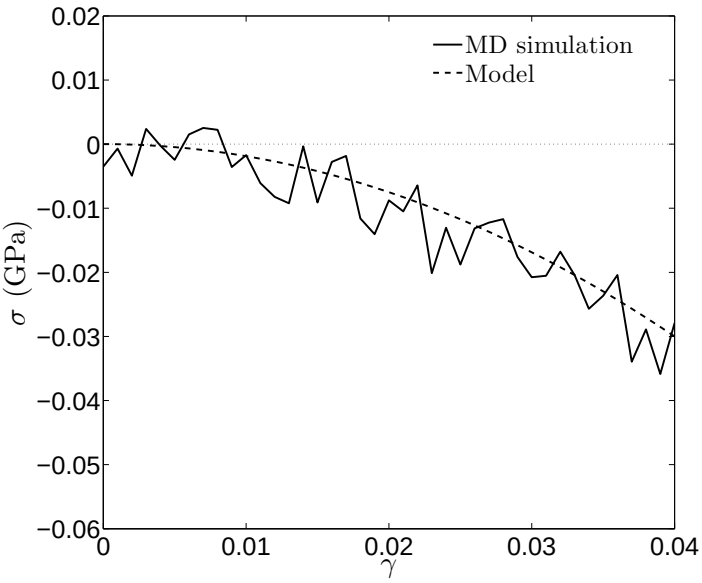

(b)

Fig. 7 Variation of (a) the shear stress and (b) the mean stress with elastic shear strain. The solid lines are the result of the MD simulations, and the dashed lines are the result of the calibrated hyperelasticity model.

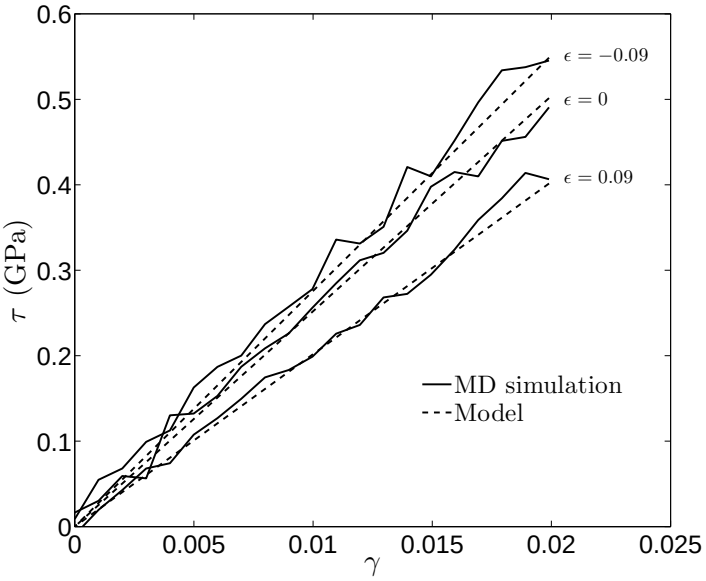

(a)

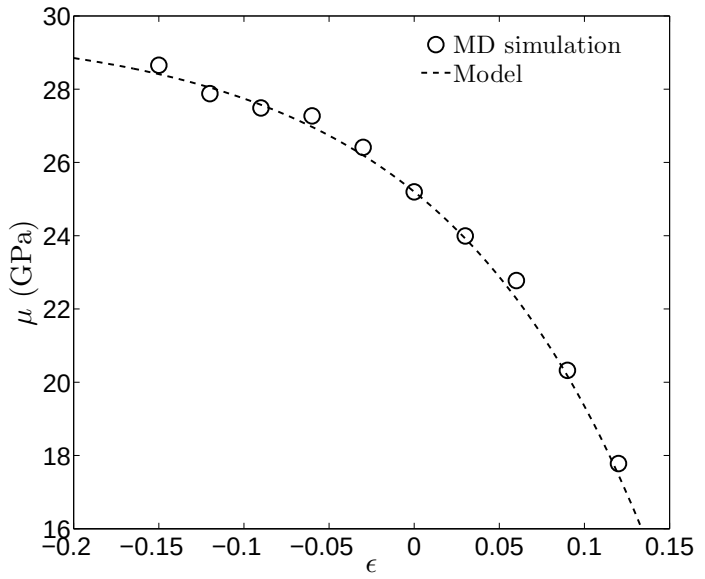

(b)

Fig. 8 (a) Variation of the shear stress with shear strain at several levels of volumetric strain and (b) variation of the shear modulus with volumetric strain. The solid lines and markers are the result of the MD simulations, and the dashed lines are the result of the calibrated hyperelasticity model.

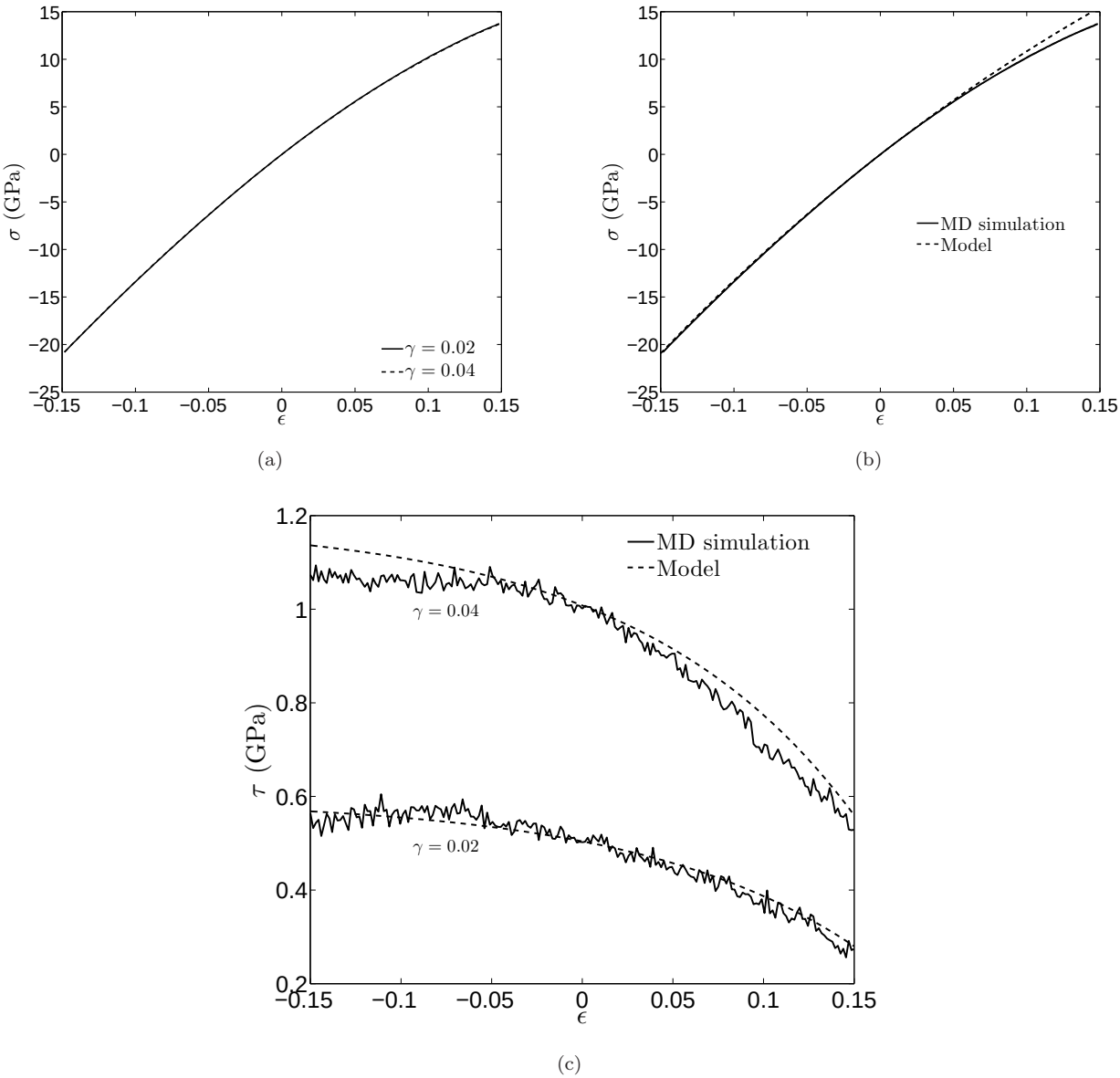

Fig. 9 (a,b) Variation of the mean stress with volumetric strain at two levels of fixed shear strain. (a) shows only the result from the MD simulations, and (b) compares the calibrated hyperelasticity model with the results of the MD simulations for both levels of fixed shear strain. (c) Variation of the shear stress with volumetric strain at two levels of fixed shear strain. In (b) and (c), the solid lines are the result of the MD simulations, and the dashed lines are the result of the calibrated hyperelasticity model.

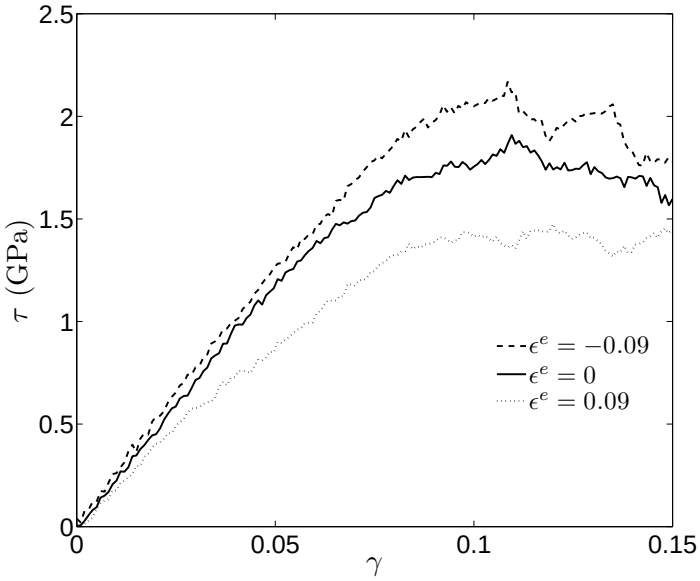

(a)

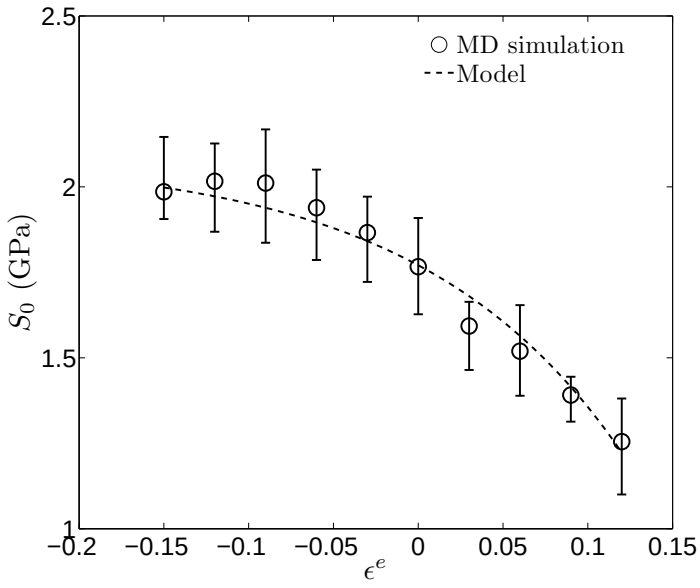

(b)

Fig. 10 (a) Variation of the shear stress with shear strain at several levels of volumetric strain, and (b) the variation of the flow stress with volumetric strain.

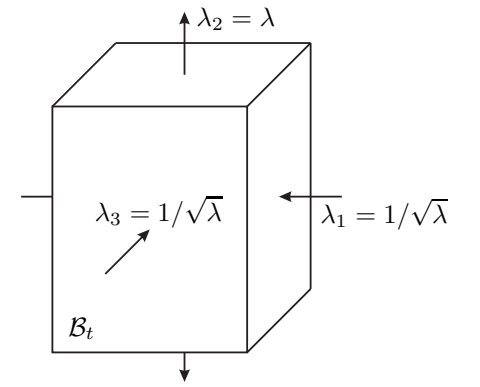

(a)

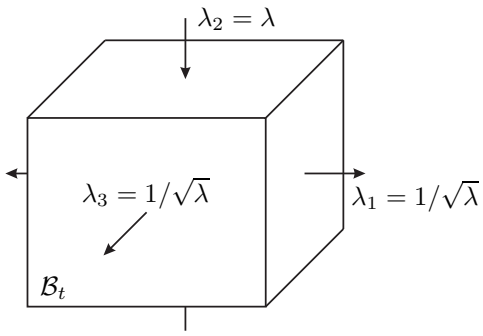

(b)

Fig. 11 Schematic of deformed configuration of the body in (a) isochoric extension, $\lambda > 1$, and (b) isochoric compression, $\lambda < 1$.

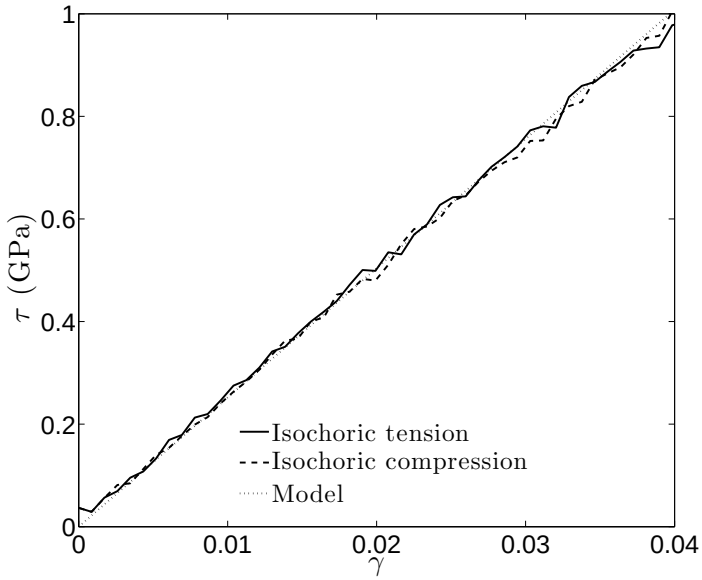

(a)

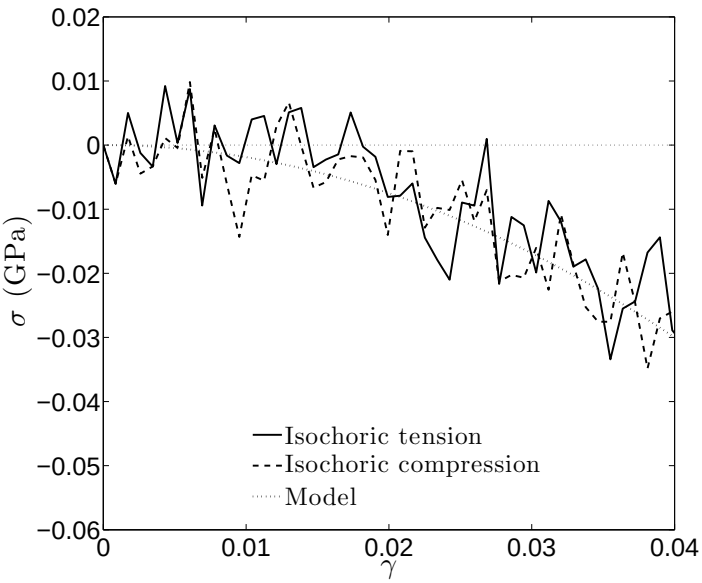

(b)

Fig. 12 Variation of (a) the shear stress and (b) the mean normal stress with elastic shear strain in iscohoric extension and isochoric compression. The solid and dashed lines are the result of the MD simulations, and the dotted lines are the result of the calibrated hyperelasticity model.